Zuse Institute Berlin

Takustr. 7
14195 Berlin
Germany

MARTIN HAMMERSCHMIDT, SANDRA DÖPKING, SVEN BURGER, SEBASTIAN MATERA

# Field Heterogeneities and their Impact on Photocatalysis: Combining optical and kinetic Monte Carlo Simulations on the Nanoscale

ZIB Report 17-20 (April 2017)

Zuse Institute Berlin
Takustr. 7
14195 Berlin
Germany

Telephone: +49 30-84185-0
Telefax: +49 30-84185-125

E-mail: bibliothek@zib.de
URL: http://www.zib.de

ZIB-Report (Print) ISSN 1438-0064
ZIB-Report (Internet) ISSN 2192-7782

# Field Heterogeneities and their Impact on Photocatalysis: Combining optical and kinetic Monte Carlo Simulations on the Nanoscale

Martin Hammerschmidt,[1, a)] Sandra Döpking,[2, b)] Sven Burger,[1, c)] and Sebastian Matera[2, d)]

[1)] *Zuse Institute Berlin, Takusstraße 7, D-14195 Berlin, Germany*

[2)] *Institute for Mathematics, Freie Universität Berlin, Arnimallee 6, D-14195 Berlin, Germany*

Gaining insights into the working principles of photocatalysts on an atomic scale is a challenging task. The obviously high complexity of the reaction mechanism involving photo-excited electrons and holes is one reason. Another complicating aspect is that the electromagnetic field, driving photocatalysis, is not homogeneous on a nanoscale level for particle based catalysts as it is influenced by the particle's shape and size.

We present a simple model, inspired by the $CO_2$ reduction on titania anatase, which addresses the impact of these heterogeneities on the photocatalytic kinetics by combining kinetic Monte Carlo with electromagnetic wave simulations. We find that average activity and especially efficiency might differ significantly between different particles. Moreover, we find sizable variation of the catalytic activity on a single facet of a nanocrystal. Besides this quantitative heterogeneity, the coverage situation in general changes laterally on this facet and we observe a concomitant change of the rate-determining steps.

This heterogeneity on all levels of photocatalytic activity is masked in experimental studies, where only the spatially averaged activity can be addressed. Microkinetic models based on experimental findings might therefore not represent the true microscopic behavior, and mechanistic conclusion drawn from these need to be handled with care.

[a)] Electronic mail: hammerschmidt@zib.de

[b)] Electronic mail: doepking@zedat.fu-berlin.de

[c)] Electronic mail: burger@zib.de

[d)] Electronic mail: matera@math.fu-berlin.de

## I. INTRODUCTION

Growing populations, advances in technology and growing consciousness for more sustainable life-styles have increased the demand not only for more energy and chemical products but also for its efficient and sustainable production using abundant materials and solar power. Efficient photocatalytic reactions are thus in high demand for many aspects of our modern life. Proposed and realized applications range from removing pollutants and pathogens from surfaces[1–4] and fluids[5] to use in other fields[6]. One area gaining ever more traction in current research is the generation of so-called "solar fuels", that is storing solar energy in chemical bonds. Solar fuels promise to contribute substantially to a renewable energy production by solving the problem of storing solar energy. Direct conversion of light without an intermediate electrolysis step to generate hydrogen has shown great promise with record conversion efficiencies[7,8]. Besides water splitting, the efficient reduction of $CO_2$ is one of most sought after reactions in the field of solar fuels[9,10]. It not only provides a means to generate storable, liquid hydrocarbons in reactions with water, but, if applied on a large scale, would also reduce the $CO_2$ content in the earth's atmosphere thus limiting the effect it has on climate change as a green house gas. Hence it is often referred to as the "holy grail" of solar fuels research[11].

Many different aspects of the photocatalytic reaction process and their interplay are to be considered when modelling the full reaction process in a semiconductor. Starting with efficient light harvesting, possibly enhanced through nanostructuring the absorber[12,13], the charges generated by the absorption of photons need to separated and to be transported to the reaction sites located at the surface of a catalyst. Subsequently, the catalytic reaction requires all the reactants to be present at the appropriate sites and the products need to be produced and transported away efficiently. This is by no means a simple modelling task. Current modelling efforts focus on understanding and improving isolated steps of the overall process and usually disregard localized effects on small scales. However, we regard an in-depth understanding of the complete photocatalytic reaction in a complex systems as an essential step in the development of efficient photocatalytic reactions for solar fuel generation. Simulation of the whole process allows to distinguish the causes and quantify the influences of different modelling parameters on the overall conversion efficiency and helps to identify limitations in this context.

In this work we present a first step in modelling the complete photocatalytic reaction chain of $CO_2$ reduction on titania anatase with consideration of nanoscale field heterogeneities and their influence on overall conversion efficiency. Similarly to our previous work on mass transfer effects is classical catalysis[14,15], we combine rigorous electromagnetic wave simulation with kinetic Monte Carlo techniques for the chemical reaction process to demonstrate the possibility to model und a study spatially resolved photocatalytic reactions on nanostructures in the gas phase. Although the presented model can only be considered a toy model as it relies on many simplifying assumptions, it demonstrates the power of studying the influence of heterogeneities in the reaction introduced by the non-uniformity of the electromagnetic field and the inherent non-linearity of the chemical processes. In particular, we address the limits of conclusions drawn from experiments in determining the details of the kinetic mechanisms and atomistic driving forces.

In section II we present the details of the model and discuss assumptions for the modelling steps of electromagnetic wave propagation, electronic species and transport as well as surface reaction kinetics and $CO_2$ reduction on anatase titania. In section III we list and discuss results of the model applied to titania anatase nanoparticles of different sizes. The observations distinguish global effects from localized field heterogeneities. Conclusions drawn and limitations of the model are addressed in section IV.

## II. A SIMPLE MODEL FOR EM-KINETIC COUPLING

In the following we present a very simplified yet powerful model to address the impact of electromagnetic field heterogeneities on the photo-catalytic activity introduced by the interaction of light with nanoscale structures such as particles. We focus on the process of $CO_2$ reduction on isolated titania anatase particles, that is the particle is only in contact with the surrounding gas phase but no other material.

The geometrical shape is chosen to minimize the surface free energy[16]. In the equilibrium shape the particles have two kinds of surface facets: the (100) and the (101) surface termination. For simplicity, we will assume that only the dominant (101) termination is photo-catalytically active. This photo-catalytic activity is driven by electrons and holes, which have been generated in the semiconductor by photon absorption. Hence, we begin the explanation of our model with the simulation of electromagnetic wave propagation and

absorption in section II A. We present our very simplified model for calculating bulk and surface electron densities in section II B and section II C, respectively. In section II D, we present a simple kinetic Monte Carlo model for the $CO_2$ reduction on anatase (101), which has been inspired by the Density Functional Theory (DFT) derived mechanism by He, Zapol, and Curtiss[17].

For our combined model, we make a simplifying feed-forward assumption: the results of each modeling step impacts the following but not vice versa. That is, we assume that bulk electrons are generated by the photon absorption, but the presence of bulk electrons has no impact on the EM-wave propagation beyond the empirical dielectric response employed in the EM simulation. Similarly, surface electrons are generated from bulk electrons, effects on the bulk electron density are neglected. We further assume that surface chemistry does not influence the surface electron density. These assumptions lead to a simple feed-forward procedure, in which the results of each step are the input for the next. In addition to this decoupling of the steps, we assume a magical, i.e. perfect co-catalyst on the surface which immediately consumes all surface holes for the production of surface protons.

### A. Electromagnetic Field Propagation

The aim of the optical modeling is to investigate the optical near fields at and just below the surface of the $TiO_2$ nanoparticle and to quantify differences in bulk and surface absorption between resonant and non-resonant excitation within the solar spectrum. The $TiO_2$ nanoparticles are modeled as axis-aligned, truncated octahedra with a single scale parameter: the side length of the square base. The height is set to 1.45 times the side length.

The scattering of monochromatic incident light by the nanoparticles is governed by the linear Maxwell's equations in frequency domain. The electric field $E$ thus solves the following second order partial differential equation

$$\nabla \times \mu^{-1} \nabla \times E - \omega^2 \varepsilon E = 0 \tag{1}$$

where $\mu$ and $\varepsilon$ are the permeability and permittivity tensors, $\omega$ is the time-harmonic frequency of the incident electromagnetic field. The finite element method[18] is a well established solution technique for the time-harmonic Maxwell's equation. It allows for extremely accurate geometrical modeling of complex 3D structures and high-accuracy electromagnetic

field solutions. The perfectly matched layer method (PML)[19,20] is used as a transparent boundary condition to avoid unphysical reflections from the truncation to a finite domain used for computations.

The surrounding medium is modeled as vacuum with $\varepsilon = \varepsilon_0 \varepsilon_r$ ($\varepsilon_r = 1$ and vacuum permittivity $\varepsilon_0$). The birefringence of $TiO_2$ is taken into account by the permittivity tensor $\varepsilon_r$ with optical constants taken from the literature[21].

The employed electromagnetic field solver JCMsuite[22,23] allows to compute multiple illuminations with different wave vectors and polarizations simultaneously. In a preliminary numerical study we thus varied the wavelength of incident plane wave illuminations as well as polarization and incidence angle to find a maximum of the electric field energy contained within a 5 nm thin layer beneath the particle's surface. This maximum for a 200 nm particle was found to be at 340 nm vacuum wavelength for Z polarized light incident along the X axis. This illumination is used for all simulations.

The photon absorption rate required in the subsequent modeling steps is given by the absorption rate of the electric field. In the time-harmonic setting this is computed from the imaginary part of the electric field energy density scaled by the frequency. Hence the photon absorption rate at a spatial point $x$ is

$$r_{\text{ph.}}(x) = -2\omega \mathfrak{Im} \left\{ \frac{1}{4} E(x) \cdot \overline{\varepsilon(x) E(x)} \right\} P_{in}^{-1} \tag{2}$$

with the power of the incoming plane wave $P_{in}$.

Figures 1 and 2 depict this spatially resolved absorption rate throughout one half of a 40 nm and a 200 nm particles in a false color plot. Additionally, the geometries of the complete particles are indicated by the bounding edges and the wave vector $k$ and the electric field polarization $E$ is shown. Each plot uses a linear color map scaled to the maximum of the absorption rate on the surface of each particle thus are not comparable quantitatively. The larger particle in figure 2 exhibits two bright spots of high electric field intensity and thus absorption just beneath the particle's surface. The direction of incidence of the illumination is best observed in this visualization. In contrast to this observation, the smaller particle shown in figure 1, exhibits maxima only on the edges between the (101) and (100) facets. Due to the sub-wavelength scale of this particle we do not observe localized maxima within the volume as for the larger particle.

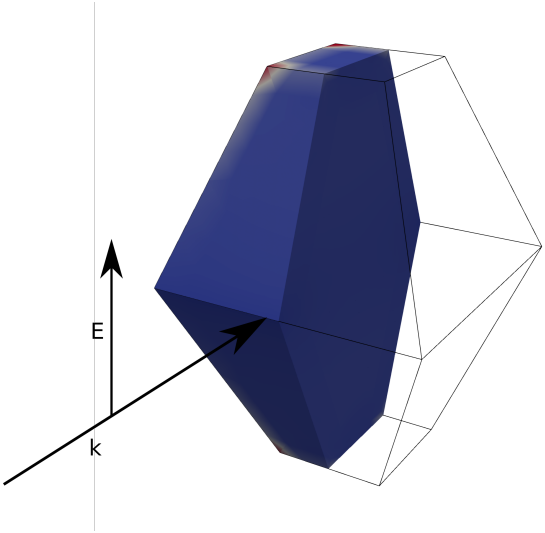


FIG. 1. Photon absorption rate for the 40 nm titania anatase nanoparticle depicted on one half of the volume. The remaining half is indicated by its bounding edges. Arrows depict the wave vector $k$ and the polarization of the electric field $E$ of the illuminating plane wave at 340 nm wavelength.

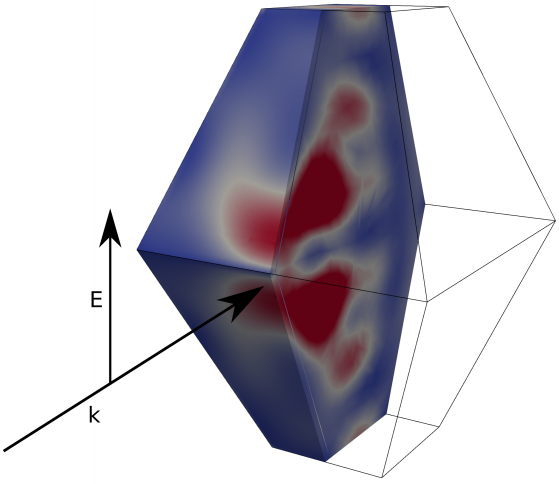


FIG. 2. Photon absorption rate for the 200 nm titania anatase nanoparticle depicted on one half of the volume. The remaining half is indicated by its bounding edges. Arrows depict the wave vector $k$ and the polarization of the electric field $E$ of the illuminating plane wave at 340 nm wavelength.

### B. Bulk electron density.

In bulk titania anatase, electrons and holes are localized on titanium and oxygen centers, respectively. Charge transport can be described by a hopping process between different

centers[24,25], albeit the simulation effort would be sizable for the considered particle sizes. Therefore, we employ a simpler phenomenological, continuum level approach where we assume that the effect of all of charge transport can be neglected compared to electron-hole pair creation and recombination. Starting without holes and electrons, this assumptions leads to equal numbers of holes and electrons in every subvolume. Having twice as many oxygen as titanium centers, the probability $p_{\mathrm{e,bulk}}$ to find an electron at a Ti center is twice the probability $p_{\mathrm{h,bulk}}$ to find a holeat an oxygen center. For each continuum point in the nanoparticle, we then approximate the electron density (or equivalently $p_{\mathrm{e,bulk}}$) using the rate equation

$$\frac{\partial p_{\mathrm{e,bulk}}}{\partial t} = r_{\mathrm{ph.}} - k_{\mathrm{recomb.}} p_{\mathrm{e,bulk}} p_{\mathrm{h,bulk}} = r_{\mathrm{ph.}} - k_{\mathrm{recomb.}} p_{\mathrm{e,bulk}} p_{\mathrm{e,bulk}}/2, \tag{3}$$

where $r_{\mathrm{ph.}}$ is the local photon absorption rate normalized per titanium atom, i.e. every photon creates an electron-hole pair. For the recombination $k_{\mathrm{recomb.}} p_{\mathrm{e,bulk}} p_{\mathrm{e,bulk}}$, we assume that the corresponding rate $k_{\mathrm{recomb.}}$ is independent of whether surrounding centers carry a charge or not. We further assumed statistical independence of all electrons and holes. We can approximate the probability of find a hole and an electron in a configuration which allows for recombination by the product $p_{\mathrm{e,bulk}} p_{\mathrm{h,bulk}}$. This meanfield assumption is justified by the relatively low charge carrier densities which we observe throughout this study. We address stationary operation and thus we find

$$\Rightarrow p_{\mathrm{e,bulk}} = \sqrt{\frac{r_{\mathrm{ph.}}}{k_{\mathrm{recomb.}}}}, \tag{4}$$

i.e. within our approximation the charge carrier density is simply proportional to the square root of the local absorption.

Electron-hole pair recombination rates $k_{\mathrm{recomb.}}$ for bulk rutile have been reported[26] to be $\approx 3 \times 10^{10}\,\mathrm{s}^{-1}$. Anatase is reported to have longer lifetimes of electron hole pairs[27] and we employ $k_{\mathrm{recomb.}} = 10^{10}\,\mathrm{s}^{-1}$. The exact value of the recombination rate, however, is actually not critical within the employed approximative model. For the electron density only the ratio $\frac{r_{\mathrm{ph.}}}{k_{\mathrm{recomb.}}}$ matters. As the Maxwell equations are linear, a smaller or higher value for $k_{\mathrm{recomb.}}$ would then be equivalent to higher or smaller applied intensity.

### C. Surface electron density.

Heterogeneous photocatalysis requires the electrons to be localized at particular surface centers for them to be utilized in the chemical elementary reactions on the surface. The electronic structure, however, changes as we approach the surface: Charge carriers might thermodynamically favor surface centers, the recombination might be faster or slower, and light absorption might be enhanced or suppressed. Thus we cannot approximate the surface probability $p_{\mathrm{e,surf.}}$ using equation (3). In the $TiO_2$(101) surface, electrons are localized at the 5-fold Ti centers, and they are significantly stronger bound to these centers than to bulk Ti centers[28]. Thus transfer of subsurface bulk electrons to the surface

$$\mathrm{e@Ti^{5+}} + \mathrm{*@Ti^{6+}} \rightarrow \mathrm{*@Ti^{5+}} + \mathrm{e@Ti^{6+}} \tag{5}$$

will contribute significantly to the number of electrons at the surface. The star $*$ indicates that the corresponding center carries no electron, i.e. the center is empty. Additionally, surface electrons might recombine with holes located at nearby bulk oxygen centers. In the mean field approximation we obtain following the approximate rate equation for the surface electron density

$$\begin{aligned}\frac{\partial p_{\mathrm{e,surf.}}}{\partial t} =& r_{\mathrm{ph.}} - k_{\mathrm{recomb.}} p_{\mathrm{e,surf}} p_{\mathrm{h,bulk}} \\ &+ k^{+}_{\mathrm{hopp.}}(1 - p_{\mathrm{e,surf}}) p_{\mathrm{e,bulk}} - k^{-}_{\mathrm{hopp.}}(1 - p_{\mathrm{e,bulk}}) p_{\mathrm{e,surf}}\end{aligned} \tag{6}$$

where we assume that $p_{\mathrm{e,surf}}$ and $p_{\mathrm{h,bulk}}$ obey the laws outlined in the previous section II B. For simplicity, we take the same electron hole pair creation $r_{\mathrm{ph.}}$ and recombination rate $k_{\mathrm{recomb.}}$ as for the bulk. We assume an ideal co-catalyst removing any surface holes immediately allowing us to neglect recombination between surface holes and electrons. The second line describes the addition ($k^{+}_{\mathrm{hopp.}}(1 - p_{\mathrm{e,surf}}) p_{\mathrm{e,bulk}}$) and removal ($k^{-}_{\mathrm{hopp.}}(1 - p_{\mathrm{e,bulk}}) p_{\mathrm{e,surf}}$) of electrons from and to the bulk by hopping. DFT based estimates for the hopping rates $k_{\mathrm{hopp.,bulk}}$ in bulk anatase have been reported to be $\approx 10^{10}\,\mathrm{s}^{-1}$ at room temperature[24]. The relative energetic stability of surface electrons to bulk electron has been estimated[28] to be $\approx 0.4\,\mathrm{eV}$. As forward and backward hopping rate should obey detailed balance, we thus have

$$k^{+}_{\mathrm{hopp.}} \approx K^{1-\alpha} k_{\mathrm{hopp.,bulk}},\ k^{-}_{\mathrm{hopp.}} \approx K^{-\alpha} k_{\mathrm{hopp.,bulk}} \text{ with } K = e^{0.4\mathrm{eV}/k_{\mathrm{B}}T} \tag{7}$$

for some value of $\alpha$ and with the Boltzmann constants $k_{\mathrm{B}}$ and the temperature $T$. We choose $\alpha = 1/2$, which corresponds to a centric placed transition state in a Brønsted-Evans-Polanyi picture[29]. As eq. (6) can be solved analytically, the surface electrons density can

easily be obtained from the simulated photon absorption rates. Note that we assumed the same energy difference between surface and bulk electrons, irrespective of what is currently adsorbed at the surface, i.e. the electronic system is completely independent of the surface chemistry.

## D. Surface kinetics modelling

### *1. Markov description of surface kinetics.*

Chemical reactions are rare events on an atomic scale, i.e. they are transitions from one metastable state in the atomic configuration space to another and the time spend within one basin is much larger than the durations of these transitions. This implies that after transitioning to a new metastable state all information about the previous state is lost. Coarse-graining the dynamics to only those metastable states allows us to regard the sequence of states as a Markov jump process.

In surface kinetics, the coarse-grained dynamics is commonly mapped on a lattice of adsorption sites at the catalyst surface. The metastable states are identified by the adsorption state of each lattice site, i.e. which kind of molecule is adsorbed on each site. A chemical elementary step will change the adsorption state of one or more close-by adsorption sites. The jump process is thus completely determined by the lattice, the possible elementary steps and the corresponding transition rates (also termed rate constants). The resulting master equation, governing the probability distribution of the metastable states, is usually too high-dimensional for a direct numerical treatment. Instead, we will employ kinetic Monte Carlo simulations to generate sample trajectories of the stochastic process, for which we employ the KMOS software package[30]. As we are interested in stationary operation, we will estimate statistical averages, like conversion rates or coverages, by time averaging.

### *2. $CO_2$ reduction model*

For modelling the surface reactivity, we want to assume that the (100) facets are inactive. For the remaining (101) facets of the considered particles, we consider a relatively simple model mechanism for the reduction of $CO_2$ to formic acid, which was motivated by the work of He, Zapol, and Curtiss on corresponding elementary pathways on (doped) anatase (101)[17].

On the (101) surface, protons $H^+$ adsorb on the twofold bridging oxygen sites, while $CO_2$, formic acid and their intermediates preferably bind to the 5-fold Ti surface atoms. These sites are arranged on the surface in alternating chains, each consisting of only one type of adsorption site. The afore mentioned ideal co-catalyst shall now have the effect to always fully populate the bridging oxygen sites with protons, in addition to the immediate removal of surface holes. In this ideal setting, the probability to find a bridging oxygen site occupied by a proton is unity and we do not need to incorporate the dynamics on the oxygen sites into our kMC model. The processes in the kMC model couple then only Ti sites on the same chain. Molecules can be adsorbed in two binding situations: i) monodentate, binding to only one Ti atom, or ii) bidentate, binding to two neighboring Ti atoms on a chain. These two configurations can easily be incorporated into a kMC model by introducing an additional (virtual) adsorption site between each pair of neighboring Ti sites. We will abbreviate these sites by B. Bidentate binding then corresponds to a (monodentate) adsorption on these B sites. The bidentate character of the binding is ensured by each adsorbed molecule blocking the neighboring sites, i.e. a molecule on a Ti sites ensures that the neighboring B sites stay empty and an adsorbate on a B site ensures that the neighboring Ti sites as well as the two nearest B sites stay empty. Such blocking rules are introduced by a proper definition of the elementary mechanism. The employed mechanism in this study is presented in table I.

It remains to assign a rate constant (RC) to each elementary step. For adsorption and desorption of $CO_2$ we follow the common approach in classical heterogeneous catalysis[31]. This means we model the adsorption RC as

$$k_{\mathrm{ad.,CO_2}} = \frac{S_{\mathrm{ad.,CO_2}} P_{\mathrm{CO_2}} A_{\mathrm{cell}}}{\sqrt{2\pi m_{\mathrm{CO_2}} k_{\mathrm{B}} T}} \tag{8}$$

where $P_{\mathrm{CO_2}}$ is the partial pressure of $CO_2$, $m_{\mathrm{CO_2}}$ is the mass of a $CO_2$ molecule, $A_{\mathrm{cell}} \approx 40\,\text{Å}^2$ is the area of the surface unit cell, and $S_{\mathrm{ad.,CO_2}}$ is the sticking probability which we assume to be unity. The desorption RC is obtained from detailed balance

$$k_{\mathrm{de.,CO_2}} = e^{-\frac{\Delta G_{\mathrm{ad.,CO_2}}}{k_{\mathrm{B}} T}} k_{\mathrm{ad.,CO_2}} \tag{9}$$

with the free energy difference $\Delta G_{\mathrm{ad.,CO_2}}$ between adsorbed and desorbed $CO_2$. We approximate the free energy difference from the adsorption energy $E_{\mathrm{ad.,CO_2}}$ as $\Delta G_{\mathrm{ad.,CO_2}} = -\Delta E_{\mathrm{ad.,CO_2}} - \mu_{\mathrm{CO_2}}$, where $\mu_{\mathrm{CO_2}}$ is the gas phase chemical potential, which we determine from tabulated experimental data[32]. We note that $CO_2$ adsorption and desorption are in

TABLE I. Elementary reaction steps, corresponding rate constant expression and parameters

| Process | rate expression | parameters |
|---|---|---|
| $CO_2(\text{gas}) + *@\text{Ti} + 2*@\text{B}$ $\rightarrow CO_2@\text{Ti} + 2*@\text{B}$ | $k_{\text{ad.},CO_2} \frac{S_{\text{ad.},CO_2} P_{CO_2} A_{\text{cell}}}{\sqrt{2\pi m_{CO_2} k_B T}}$ | $A_{\text{cell}} = 41.25\,\text{Å}^2$, $S_{\text{ad.},CO_2} = 1$ |
| $CO_2@\text{Ti}$ $\rightarrow CO_2(\text{gas}) + *@\text{Ti}$ | $k_{\text{de.},CO_2} = e^{\frac{\Delta E_{\text{ad.},CO_2} + \mu_{CO_2}}{k_B T}} k_{\text{ad.},CO_2}$ | $\Delta E_{\text{ad.},CO_2} = 0.4\,\text{eV}$ |
| $\text{HCOOH}@\text{Ti}$ $\rightarrow \text{HCOOH(gas)} + *@\text{Ti}$ | $\frac{k_B T}{h} e^{-\frac{\Delta E}{k_B T}}$ | $\Delta E = 0.7\,\text{eV}$ |
| $CO_2@\text{Ti} + *@\text{Ti} + 2*@\text{B} + e_{\text{surf.}}$ $\rightarrow 2*@\text{Ti} + *@\text{B} + CO_2^-@\text{B}$ | $\frac{k_B T}{h} e^{-\frac{\Delta E}{k_B T}} p_{\text{e,surf.}}$ | $\Delta E = 0.67\,\text{eV}$ |
| $*@\text{Ti} + *@\text{B} + CO_2^-@\text{B}$ $\rightarrow CO_2@\text{Ti} + 2*@\text{B} + e_{\text{surf.}}$ | $\frac{k_B T}{h} e^{-\frac{\Delta E}{k_B T}} (1 - p_{\text{e,surf.}})$ | $\Delta E = 0.43\,\text{eV}$ |
| $CO_2@\text{Ti} + 2e_{\text{surf.}} + H^+$ $\rightarrow \text{HCOO}^-@\text{Ti}$ | $\frac{k_B T}{h} e^{-\frac{\Delta E}{k_B T}} p_{\text{e,surf.}}^2$ | $\Delta E = 1.11\,\text{eV}$ |
| $CO_2^-@\text{B} + e_{\text{surf.}} + H^+$ $\rightarrow \text{HCOO}^-@\text{B}$ | $\frac{k_B T}{h} e^{-\frac{\Delta E}{k_B T}} p_{\text{e,surf.}}$ | $\Delta E = 0.01\,\text{eV}$ |
| $\text{HCOO}^-@\text{Ti} + H^+$ $\rightarrow \text{HCOOH}@\text{Ti}$ | $\frac{k_B T}{h} e^{-\frac{\Delta E}{k_B T}}$ | $\Delta E = 0.01\,\text{eV}$ |
| $CO_2^-@\text{B} + *@\text{Ti} + H^+$ $\rightarrow \text{HCOOH}@\text{Ti} + *@\text{B}$ | $\frac{k_B T}{h} e^{-\frac{\Delta E}{k_B T}}$ | $\Delta E = 0.46\,\text{eV}$ |

equilibrium for all cases, we have investigated. Hence, the detailed choices for the sticking probability and the unit cell size have no impact on the simulation results.

All other reactions do not involve gas phase species and most can be cast into the general reaction equation

$$\sum_{\text{A}} \nu_{\text{A,Ti}} \text{A}@\text{Ti} + \sum_{\text{A}} \nu_{\text{A,B}} \text{A}@\text{B} + \nu_{\text{H}^+} \text{H}^+ + \nu_e e_{\text{surf.}} \rightarrow ... \tag{10}$$

where the sums run over all possible adsorbates on Ti and B, respectively. The RC for such reactions are modeled as

$$k = \frac{k_B T}{h} e^{-\frac{\Delta E}{k_B T}} p_{\text{e,surf.}}^{\nu_e} \tag{11}$$

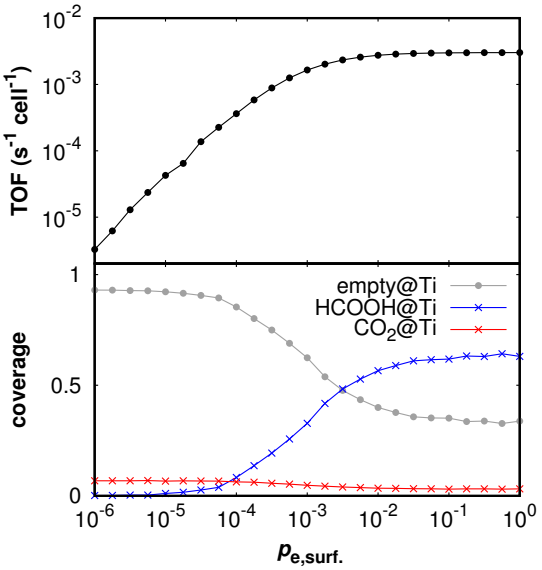


FIG. 3. Turnover-frequencies (TOF) and coverages as function of the surface electron density $p_{\mathrm{e,surf.}}$.

where $h$ is Planck's constant and $\Delta E$ is the energy barrier for this reaction. In equation (11) we exploited the meanfield assumption for the electron treatment. For reactions which do not consume surface electrons, but release them the factor $p_{\mathrm{e,surf.}}^{\nu_e}$ must be replaced with $(1 - p_{\mathrm{e,surf.}})^{\nu_r}$ where $\nu_r$ is the number of electrons released in this step. This reflects, that for such reactions to take place, there must be empty centers for the released electrons.

Within our approximative model the surface electron density is not affected by the dynamics on the surface, such that $p_{\mathrm{e,surf.}}$ is a simple parameter on the kMC level. The probability to find a proton does not appear in eq. (11) as we assumed it to be unity. In a meanfield picture deviations from unity would be incorporated by a power law dependence, as we have done for $p_{\mathrm{e,surf.}}$.

The employed elementary steps, their rate expressions and corresponding rate parameters are provided in table I. Note, that those reactions which involve protons as reactants are irreversible, as the assumed ideal co-catalyst refills the empty oxygen sites and the reverse reaction cannot happen. The employed mechanism and its parameters must be considered a toy model, albeit they are inspired by the DFT derived mechanism and barriers from ref.[17], especially those for the zirconium doped titania surface.

Figure 3 shows the kMC simulation results for the outlined model at one atmosphere

$CO_2$ partial pressure, $T = 300\,\mathrm{K}$ and varying surface electron density $p_{\mathrm{e,surf.}} \in [10^{-6}, 1]$. All simulations have been run on a lattice of $20\mathring{A} \times 20\mathring{A}$ surface unit cell with periodic boundary conditions and $10^9$ kMC steps for initial relaxation as well as the same number for sampling stationary expected values. The upper panel shows the turnover frequency (TOF), i.e. the number of formic acid molecules desorbing from the surface per unit time and surface unit cell. The lower panel shows the average coverage of $CO_2$@TI, HCOOH@TI or empty @TI. As expected, the TOF increases monotonously with $p_{\mathrm{e,surf.}}$, but the TOF curve flattens between $p_{\mathrm{e,surf.}} = 10^{-4}$ and $p_{\mathrm{e,surf.}} = 10^{-2}$. Above $p_{\mathrm{e,surf.}} = 10^{-2}$, the TOF is almost independent of the electron density. This indicates a change of the rate-determining steps, identified by the Degree of Rate Control[33,34], when increasing $p_{\mathrm{e,surf.}}$. This is reflected in the coverage plot in the lower panel of figure 3. At low $p_{\mathrm{e,surf.}}$, the surface is almost empty with $\approx 10\,\%$ $CO_2$ occupation of the Ti sites. The change in the slope of the TOF curve is accompanied by an increase of the formic acid coverage and, at high $p_{\mathrm{e,surf.}}$, formic acid accumulate at the surface. Therefore the rate-limiting step is no longer one of the reactions which require surface electrons to produce formic acid, but the actual desorption of formic acid from the surface.

## III. RESULTS

We now turn to the combination of the models outlined in the previous section II. For this we use the FEM simulation of the electromagnetic field to obtain the spatially resolved photon absorption rate $r_{\mathrm{ph.}}$ with the help of eq. (2). This field is then used to determine the fields of bulk electron density and surface electron density via equations (3) and (6). The latter field serves as input for the surface kinetics. In practice, we interpolate the data in figure 3, such that the laterally resolved TOFs and coverages can efficiently be obtained.

We simulated two particles differing only in size (200 nm and 40 nm side length and heights of 290 and 58 nm, respectively). As mentioned above, we impose identical illumination for observed differences to result solely from the scale of the particles. This scale was chosen to shift the resonance wavelength of the larger particle into the narrow region where the absorption spectrum of $TiO_2$ and the solar spectrum overlap. Instead of using the whole solar spectrum we focus the discussion on the results for a single wavelength of 340 nm.

We first analyse the catalytic activity on a global scale before focussing on local obser-

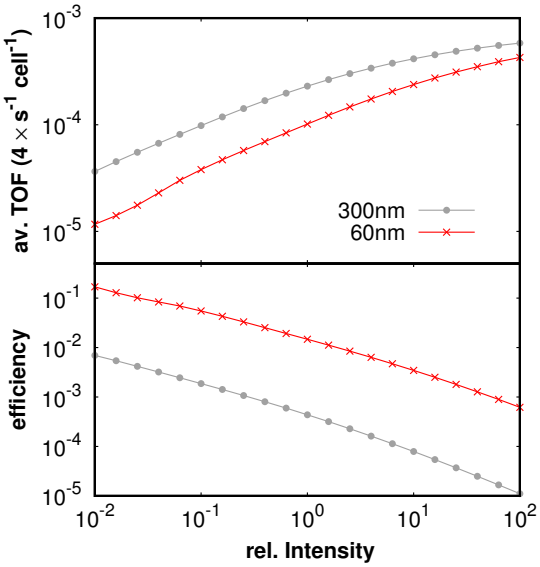


FIG. 4. Turnover-frequencies (TOF) and efficiency as function of applied illumination.

vations in section III B.

## A. Global behaviour

We first investigate the global response of the two investigated particles to the applied illumination, whose intensity we measure in multiples of the solar irradiance at the employed wavelength of 340 nm. A central objective is the laterally averaged TOF, i.e. the integral of the TOF over the particle surface divided by the surface area. On the other hand, efficiency of the particles for conversion of absorbed photons to reaction products is equally important. This efficiency is best measured by the surface integral of the TOF divided by the (volumetric) integral absorption rate. Both, average TOF and efficiency, are displayed in figure 4 for the two particles and a $CO_2$ partial pressure of one bar and $T = 300\,\mathrm{K}$. The average activity for both particles increases with the illumination while the efficiency decreases. The increase in average activity is a consequence of the higher photon absorption and thereby higher electron and hole densities at increased illumination. However, at increased charge carrier densities, created electrons and holes are more likely to recombine. Thus a larger fraction of the created electron hole pairs will recombine before they can be utilized in a surface reaction and the efficiency must therefore drop. Besides this common qualitative behavior, the 200 nm particle shows the higher average activity than the smaller 40 nm par-

ticle, but it also has a significantly lower efficiency. A common explanation for the higher efficiency of smaller particles is the shorter diffusion length for a charge carrier to reach the surface. Within our model, this cannot explain the observed effect, because we have explicitly neglected charge carrier transport. Rather, this behavior results from the differences of in photon absorption in the two particles. Partly, the difference might be explained by the lower average photon absorption rate for the smaller particle. The argument would then be similar as for the illumination dependence of the efficiency: the charge carrier density and therefore recombination is lower leading to a higher efficiency. A closer look at the spatially resolved absorptions in the figures 1 and 2 indicates that this interpretation is probably oversimplified. The three-dimensional absorption field of the larger particle is not just the enlarged version of the absorption field for the smaller particle, but shows a qualitatively different behavior. For the smaller particle electron-hole pairs are primarily created in the vicinity of the edges between the (101) and (100) facets, i.e. close to the reactive surface. These electrons close to the surface are more likely to take part in the surface reactions and this results in a relatively high efficiency. In contrast, we also observe high absorption in the volume of the larger particle below the surface. Within our model, the created electron hole pairs in the volume cannot trigger a surface reaction and will therefore recombine, thus reducing the overall efficiency.

### B. Locally resolved response

For solar illumination, the relevant fields on the reactive (101) facets are shown in figures 5 and 6 for the large and the small particle, respectively. The facets facing the incoming photons are displayed to the left, followed by one of the sides. The third truncated rhombus represents the backside and the far right shows the remaining side. Both particles show a significant lateral variation of the photon absorption rate. This heterogeneity transfers to the density of surface electrons and finally to the lateral distribution of the TOF. Notably, the peak TOF does not differ much between both particles. The larger average TOFs for the larger particle rather result from the larger fraction of the surface showing significant light absorption and thereby a significant electron density and TOF. These significant quantitative lateral variations go hand in hand with qualitative changes in the surface chemistry, which manifests in the formic acid coverage in the lowest panel. This coverage varies between

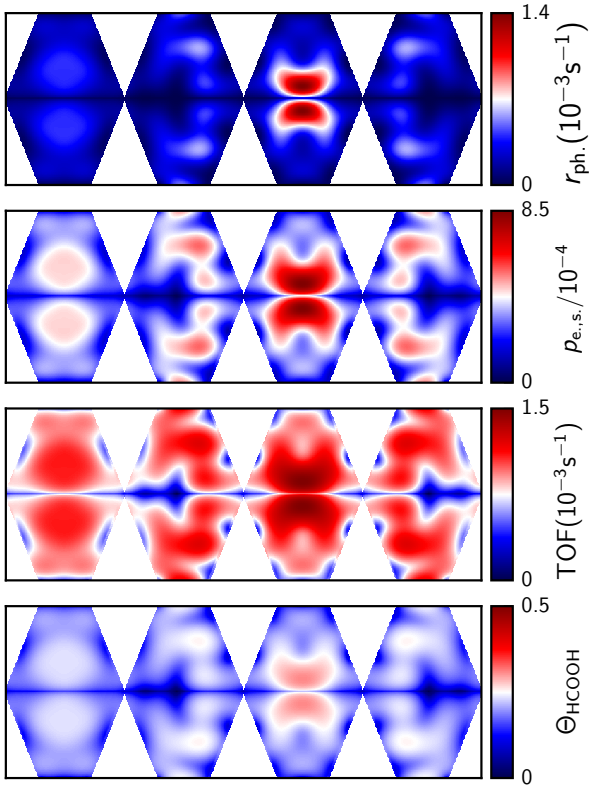


FIG. 5. detailed distribution of TOF coverages, absorption rate, electron density for large particle at solar illumination.

almost zero and a finite value of $\approx 0.3$. This is more prominently seen in case of the larger particle, but also the smaller particle shows high HCCOH coverages in the corners. As outlined in section II D, non-vanishing HCOOH coverages indicate that the formic acid desorption becomes rate-limiting. We thus have parts of the surface, where this step is rate-limiting (high HCOOH coverage), while in other parts this step is unimportant (low HCOOH coverage).

### C. Discussion

The two investigated problems are idealized, well controlled situations and differ only by the size of the particle. Still we find large deviations between both and a strong nano-scale heterogeneity on their surfaces. Our study implies, that other properties like shape and orientation have a similar impact on the light absorption. Our results illustrate the difficulties, when trying to understand photo-catalysis on structured catalysts even in such

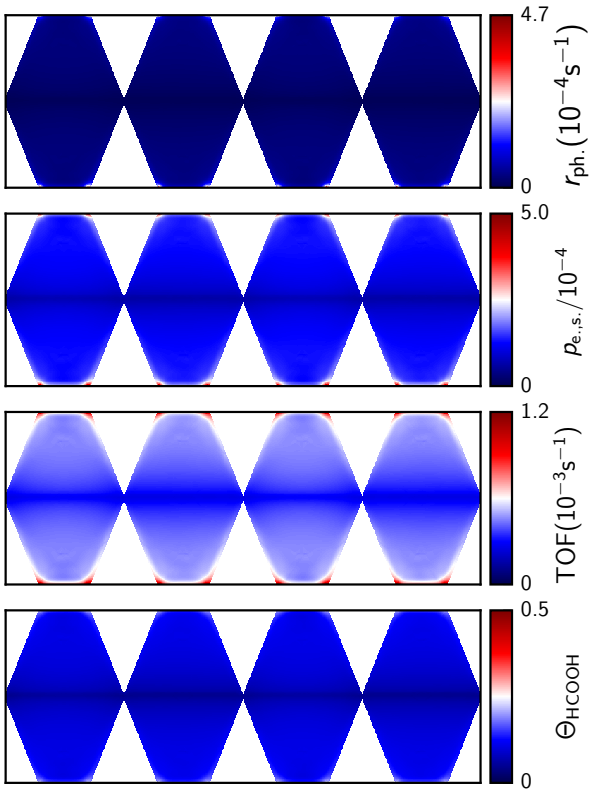


FIG. 6. detailed distribution of TOF coverages, absorption rate, electron density for small particle at solar illumination.

idealized settings. The active facets of the larger particle have a high HCOOH coverage, while only the corners of the smaller particle show a similar coverage. In both cases, we additionally find strong lateral heterogeneities of the TOF and the coverage on a single facet. Such effects challenge the analysis of experiments where only the average activity is accessible. Of course, the details of the TOF distribution cannot be determined from this observable which depends on the interplay of many different phenomena. Phenomenological microkinetic models derived from experimental observations will necessarily also represent the non-kinetic part of the activity. While such models are definitely the best choice for reactor modeling, the question arises how much information about the kinetic mechanism and on the atomistic driving forces behind the observed activity can be drawn from these models.

Our model depends on several crucial approximations. We therefore regard it as at toy model and not as a realistic model for the $CO_2$ reduction on titania anatase. We employ only a reduced mechanism with just HCOOH as product and without a dependence of the

energetics on the presence of a surface electron or the adsorption states on the surrounding sites. Other pathways and other products are known for this system[17,35] and the presence of a surface electron is likely to affect the energetics. The assumed ideal co-catalysts, immediately consuming all surface holes and delivering protons whenever needed, removes all limitations, which in reality might arise from the part of the mechanism creating protons and transporting them to the active sites for $CO_2$ reduction. These simplifications definitely affect the results of the microkinetic modeling. The reality is even more involved than outlined in section II D, especially as there are many competing reaction pathways. However, the findings that TOFs as well as coverages might significantly vary between particles and on single facets will not be affected by details of the reaction mechanism.

We also treat the electrons only with a very simplified model, neglecting e.g charge transport. In general, charge carrier densities depend on the interaction of transport, creation and recombination of electron hole pairs and trapping in surface states. This might lead to a smoothing of the charge carrier distribution and thereby to a more homogenous TOF on the surface of a single particle, compared to our present model. On the other hand, we still expect significant differences in the efficiency of both particles, as this is largely governed by the light absorption. Indeed, the effect could be enhanced by the shorter distances to the surface for bulk electrons in smaller particles. We have neglected transport not only to obtain a simpler model but to disentangle optical and transport effects as well. Properly incorporating charge transport will require an additional simulation step and will be subject of a subsequent study.

Contrary to our toy problems, real life catalysts are mixtures of many different particles with a range of sizes, shapes and orientations[36] and also usually do not operate at only a single particular wavelength. The afore mentioned difficulties in understanding the driving forces behind thereby potentiate, because different observations might be governed by very different particles with their own heterogeneous light absorption distribution and therefore reactivity. Also, particles are usually not well isolated from each other, such that the incident electromagnetic field is influenced by the presence of the neighboring particles and the nearfields might interact. Thus even two identical particles (size, shape, orientation) might show a different behavior due to their local environment. Admittedly, commonly employed titania catalysts employ particles, which are smaller than our larger particle. However, particles in real-life catalysts are never isolated. They easily lump together forming super-

structures in the size range of our larger particle. Thereby resonant effects, as we observe for the larger particle, might very well also be present in real-life catalysts.

## IV. CONCLUSIONS

We have presented a simple model to address the impact inhomogeneous of light absorption on the photo-catalytic activity on semiconductor particles. We have investigated two different situations, which differed only in the size of the considered particle. We found that the catalytic activity and especially efficiency is significantly different on both particles. Under the made assumptions, we further found that catalytic activity but also the qualitative kinetic behavior show substantial lateral variations on a single facet of a particle. Both challenges the interpretation of experimental results of photocatalysts composed of such nanoparticles.

Albeit our model aims to simulate $CO_2$ reduction on titania anatase, it requires a number of approximations to be computationally feasible and is therefore to be regarded as a toy model. Future work in this direction will concentrate on extending this model to hitherto neglected aspects, such as charge carrier transport and additional reaction products and elementary steps.

## ACKNOWLEDGMENTS

The results were obtained at the Berlin Joint Lab for Optical Simulations for Energy Research (BerOSE) of Helmholtz-Zentrum Berlin für Materialien und Energie, Zuse Institute Berlin and Freie Universität Berlin. This research was carried out in the framework of MATHEON supported by Einstein Foundation Berlin through ECMath within subprojects SE6 and SE14.

## REFERENCES

[1]H. Nakamura, M. Tanaka, S. Shinohara, M. Gotoh, and I. Karube, Biosensors and Bioelectronics **22**, 1920 (2007).

[2]J. A. Byrne, P. S. M. Dunlop, J. W. J. Hamilton, P. Fernández-Ibáñez, I. Polo-López, P. K. Sharma, and A. S. M. Vennard, Molecules **20**, 5574 (2015).

[3]R. Shirai, T. Miura, A. Yoshida, F. Yoshino, T. Ito, M. Lee, M. Yoshinari, and Y. Yajima, Clinical Oral Implants Research **25**, 179 (2014).

[4]S. Banerjee, D. D. Dionysiou, and S. C. Pillai, Applied Catalysis B: Environmental **176-177**, 396 (2015).

[5]T. Kamegawa, Y. Ishiguro, H. Seto, and H. Yamashita, J. Mater. Chem. A **3**, 2323 (2015).

[6]V. Augugliaro, G. Camera-Roda, V. Loddo, G. Palmisano, L. Palmisano, J. Soria, and S. Yurdakal, Journal of Physical Chemistry Letters **6**, 1968 (2015).

[7]F. F. Abdi, L. Han, A. H. M. Smets, M. Zeman, B. Dam, and R. van de Krol, Nature communications **4**, 2195 (2013).

[8]M. M. May, H.-J. Lewerenz, D. Lackner, F. Dimroth, and T. Hannappel, Nature Communications **6**, 8286 (2015), arXiv:1508.01666.

[9]D. Kim, K. K. Sakimoto, D. Hong, and P. Yang, Angewandte Chemie (International ed. in English) **54**, 3259 (2015).

[10]C. Kim, H. S. Jeon, T. Eom, M. S. Jee, H. Kim, C. M. Friend, B. K. Min, and Y. J. Hwang, Journal of the American Chemical Society **137**, 13844 (2015), arXiv:9809069v1 [arXiv:gr-qc].

[11]H. Tüysüz and C. K. Chan, eds., *Solar Energy for Fuels*, Topics in Current Chemistry, Vol. 371 (Springer International Publishing, Cham, 2016).

[12]F. F. Abdi, A. Dabirian, B. Dam, and R. van de Krol, Physical chemistry chemical physics : PCCP , 15272 (2014).

[13]J. Zhang, X. Jin, P. I. Morales-Guzman, X. Yu, H. Liu, H. Zhang, L. Razzari, and J. P. Claverie, ACS Nano **10**, 4496 (2016), arXiv:arXiv:1408.1149.

[14]S. Matera, M. Maestri, A. Cuoci, and K. Reuter, ACS Catalysis **4**, 4081 (2014), http://dx.doi.org/10.1021/cs501154e.

[15]S. Matera, S. Blomberg, M. J. Hoffmann, J. Zetterberg, J. Gustafson, E. Lundgren, and K. Reuter, ACS Catalysis **5**, 4514 (2015), http://dx.doi.org/10.1021/acscatal.5b00858.

[16]A. S. Barnard, J. Mater. Chem. A **3**, 60 (2015).

[17]H. He, P. Zapol, and L. A. Curtiss, Energy Environ. Sci. **5**, 6196 (2012).

[18]P. Monk, *Finite Element Methods for Maxwell's Equations*, Numerical Mathematics and Scientific Computation (Clarendon Press, 2003).

[19]J.-P. Berenger, Journal of Computational Physics **114**, 185 (1994).

[20]L. Zschiedrich, *Transparent boundary conditions for Maxwells equations: numerical con-*

*cepts beyond the PML method*, Phd thesis, Freie Universität Berlin (2009).

[21]G. E. Jellison, L. A. Boatner, J. D. Budai, B.-S. Jeong, and D. P. Norton, Journal of Applied Physics **93**, 9537 (2003).

[22]J. Pomplun, S. Burger, L. Zschiedrich, and F. Schmidt, Physica Status Solidi (B) **244**, 3419 (2007), arXiv:0711.2149.

[23]JCMsuite, *version 3.6.1* (JCMwave GmbH, Berlin, Germany, 2017).

[24]N. A. Deskins and M. Dupuis, Phys. Rev. B **75**, 195212 (2007).

[25]N. A. Deskins and M. Dupuis, The Journal of Physical Chemistry C **113**, 346 (2009), http://dx.doi.org/10.1021/jp802903c.

[26]R. Katoh, M. Murai, and A. Furube, Chemical Physics Letters **461**, 238 (2008).

[27]J. Zhang, P. Zhou, J. Liu, and J. Yu, Phys. Chem. Chem. Phys. **16**, 20382 (2014).

[28]C. Di Valentin and A. Selloni, The Journal of Physical Chemistry Letters **2**, 2223 (2011), http://dx.doi.org/10.1021/jz2009874.

[29]L. G. Arnaut, S. J. Formosinho, and H. Burrows, *Chemical kinetics: from molecular structure to chemical reactivity* (Elsevier, 2006).

[30]M. J. Hoffmann, S. Matera, and K. Reuter, Comp. Phys. Comm. **185**, 2138 (2014).

[31]K. Reuter and M. Scheffler, Phys. Rev. B **73**, 045433 (2006).

[32]Analytical Chemistry **63**, 252A (1991), pMID: 22775114, http://dx.doi.org/10.1021/ac00004a736.

[33]C. T. Campbell, Top. Catal. **1**, 353 (1994).

[34]M. J. Hoffmann, F. Engelmann, and S. Matera, J. Chem. Phys. **146**, 044118 (2017).

[35]A. Dhakshinamoorthy, S. Navalon, A. Corma, and H. Garcia, Energy Environ. Sci. **5**, 9217 (2012).

[36]J. Schneider, M. Matsuoka, M. Takeuchi, J. Zhang, Y. Horiuchi, M. Anpo, and D. W. Bahnemann, Chem. Rev. **114**, 9919 (2014).